AGU PUBLICATIONS

Geophysical Research Letters

RESEARCH LETTER
10.1002/2016GL069494

Key Points:
- Archival data show that tidal range has approximately doubled in Wilmington (NC) over the past century
- Modeling suggests that the worst-case CAT-5 storm surge increased by 40–60% since the nineteenth century
- Increased channel depths are the primary cause of altered tidal and surge wave dynamics

Supporting Information:
- Supporting Information S1

Correspondence to:
R. Familkhalili,
rfa2@pdx.edu

Citation:
Familkhalili, R., and S. A. Talke (2016), The effect of channel deepening on tides and storm surge: A case study of Wilmington, NC, *Geophys. Res. Lett.*, *43*, doi:10.1002/2016GL069494.

Received 11 MAY 2016
Accepted 15 AUG 2016
Accepted article online 17 AUG 2016

The effect of channel deepening on tides and storm surge: A case study of Wilmington, NC

R. Familkhalili[1] and S. A. Talke[1]

[1]Department of Civil and Environmental Engineering, Portland State University, Portland, Oregon, USA

Abstract In this study we investigate the hypothesis that increasing channel depth in estuaries can amplify both tides and storm surge by developing an idealized numerical model representing the 1888, 1975, and 2015 bathymetric conditions of the Cape Fear River Estuary, NC. Archival tide gauge data recovered from the U.S. National Archives indicates that mean tidal range in Wilmington has doubled to 1.55 m since the 1880s, with a much smaller increase of 0.07 m observed near the ocean boundary. These tidal changes are reproduced by simulating channel depths of 7 m (1888 condition) and 15.5 m (modern condition). Similarly, model sensitivity studies using idealized, parametric tropical cyclones suggest that the storm surge in the worst-case, CAT-5 event may have increased from 3.8 ± 0.25 m to 5.6 ± 0.6 m since the nineteenth century. The amplification in both tides and storm surge is influenced by reduced hydraulic drag caused by greater mean depths.

1. Introduction

Hurricane storm surges, the long-period wave generated by tropical cyclones, have historically produced many devastating floods along the U.S. East Coast [*Ludlam*, 1963]. As sea level increases due to climate change and other factors, the same storm surge produces larger extreme water levels (relative to a fixed datum), exacerbating this flood hazard [e.g., *Kemp and Horton*, 2013]. There is some concern that climate change may be increasing the frequency of storms and/or the magnitude of storm surge independently of sea level rise [e.g., *Holland and Webster*, 2007; *Grinsted et al*., 2012; *Lin et al*., 2012], though gaps in the historical record complicate interpretation of secular trends [e.g., *Landsea et al*., 2010]. Recent studies also suggest that local changes to bathymetry may produce changes in storm surge magnitudes over decadal and century time scales [*Talke et al*., 2014; *Orton et al*., 2015]. Similarly, changes to wetland areas are known to influence flood hazard [e.g., *Wamsley et al*., 2010]. Since much of the densely populated Atlantic coastline lies less than 3 m above mean sea level [*Climate Change Science Program Synthesis and Assessment Product 4-7*, 2008], assessing and explaining long-term changes to storm surge is vitally important.

In this study we test the hypothesis that bathymetric changes, in particular the increased depth and width caused by dredging and channel modification, can cause long-term changes to the magnitudes of storm surge and storm tides (the sum of the meteorological surge and the astronomical tide) within harbors and estuaries. Further, since both storm surge and astronomical tides are "long waves" (long wavelength compared to water depth), we hypothesize that both will be similarly affected by altered bathymetry. If correct, this implies that regions with secular shifts in tidal amplitudes [see, e.g., *Woodworth*, 2010] may also be locations with altered storm surge characteristics. Hence, the opportunity exists to investigate secular changes in storm surge using the tools, methods, and results of tidal analysis.

Though the effects of storm characteristics (e.g., wind velocity) and surge/tide interactions have been investigated by numerical models [e.g., *Peng et al*., 2004; *Shen et al*., 2006], the effect of decadal and secular changes in bathymetry has received much less attention [*Orton et al*., 2015]. By contrast, the dependency of tides on depth, cross-sectional area, convergence, and other bathymetric properties have long been investigated using idealized models [e.g., *Friedrichs and Aubrey*, 1994; *Jay*, 1991; *Lanzoni and Seminara*, 1998; *Prandle*, 2003]. These studies show that tidal amplitudes decrease upriver when frictional effects dominate over the funneling effect caused by decreasing width; by contrast, strong width convergence can produce increasing amplitude when friction is relatively weak. Significantly, the frictional damping in the linearized tidal equations is proportional to bottom roughness but inversely proportional to water depth [*Friedrichs and Aubrey*, 1994]. Therefore, over long time scales, depth changes to estuaries can significantly alter the balance of inertial effects, friction, and convergence, leading to altered tidal amplitudes. When combined

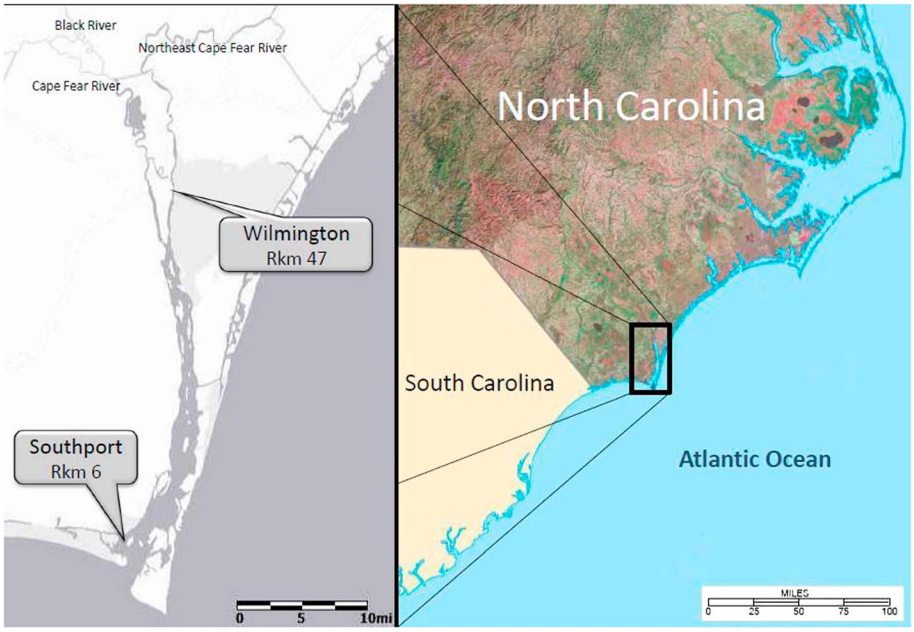

Figure 1. Cape Fear River Estuary (USGS, The National Map, http://www.nationalatlas.gov) and tide gage locations at Wilmington (NOAA Station ID: 8658120) and Southport (NOAA Station ID: 8659084).

with resonance effects, reduced friction has been observed to increase tidal range by more than 3 m at the landward end of some estuaries [*Chernetsky et al*., 2010; *Talke and Jay*, 2013].

Globally, tides in most estuaries and harbors show evidence of secular trends [*Woodworth*, 2010]. On the U.S. East Coast, Wilmington (NC) has experienced an anomalously large increase in tidal constituents and tidal range since at least 1935 [*Woodworth*, 2010]. Over the past 150 years, multiple projects in the Cape Fear River Estuary (CFRE) have approximately doubled the depth of the shipping channel between the ocean and Wilmington (at ~ Rkm 47) [e.g., *USACE COE*, 1873, 1915; *Welch and Parker*, 1979; *Olsen*, 2012]. Combined with its documented vulnerability to flooding from tropical cyclones (TCs) [*Xia et al*., 2008], the CFRE is an ideal location to test the hypothesis that depth changes can produce large alterations to both tides and storm surge. Moreover, because the CFRE approximates a funnel-shaped estuary between Rkm 12 and 50, idealized tidal theory [*Jay*, 1991; *Friedrichs and Aubrey*, 1994] can be used to interpret secular changes.

In this contribution we recover and use archival tide and bathymetric data from as early as 1888 to investigate how CFRE tidal dynamics are affected by channel depth and width changes. Because much of the estuary approximates a funnel-shaped geometry, an idealized modeling approach to understand first-order system physics and sensitivities is justified (see supporting information). In turn, a parametric model of hurricane wind and pressure forcing is applied to the idealized bathymetry to determine how broadband long waves react to secular changes in depth. Results suggest a simple but profound lesson: locations in which tide waves have been amplified are also vulnerable to increases in storm surge and flood risk, to a degree that is related to changed tidal dynamics.

2. Methods

2.1. Study Domain

The Cape Fear River (NC) is a 322 km river with a watershed of 23,581 km^2 and a discharge that varies between ~10 and 3800 m^3/s, with an average annual flow of ~270 m^3/s. Two tributaries, the Black River and the Northeast Cape Fear River, combined with the main stem at Rkm 70 and 47 (Figure 1). Tides propagate about 100 km upstream from the estuary mouth (Rkm 0) [*Giese et al*., 1985]. Like many river estuaries on the East Coast and worldwide (e.g., the Delaware) [see *Lanzoni and Seminara*, 1998], the CFRE is approximately funnel shaped over a large part of its domain.

Wilmington, a significant port, is located at approximately Rkm 47 (Figure 1). In the midnineteenth century, the controlling depth at the bar (Rkm 0) and in the estuary varied between 3 and 5 m relative to mean low water (MLW) [*USACE COE*, 1873]. Initial efforts to control flow began in the 1820s, but large-scale diking and jetty construction only began around 1870, with significant dredging beginning in 1881 [*USACE COE*, 1915]. Continued work increased the channel depth to 9.1 m by 1932, 11.6 m by 1971, and 13.5 m by 2001, relative to MLW [*Welch and Parker*, 1979; *Olsen*, 2012]. The inlet width and channel width were widened to ~120 and 90 m in 1913, from ~80 m in the 1880s [*Welch and Parker*, 1979]. The modern (2015) shipping channel is maintained at a depth of 15.5 m relative to MSL (14.8 m relative to MLW) and a width of 180 m.

Significant tropical cyclones have also impacted the region near the CFRE over the past 100 years. The most intense, Hurricane Hazel (1954) and Hurricane Fran (1996), made landfall as CAT-4 and CAT-3 hurricanes, respectively, producing 0.96 m and 1.7 m surge at Wilmington. Other significant surge events include an unnamed 1944 event (0.72 m surge), an unnamed 1945 event (0.66 m), Hurricane Floyd (1999; 1.14 m), Hurricane Charley (2004; 1.39 m), and Hurricane Hanna (2008; 1.47 m). Qualitatively, these hurricane storm surge magnitudes were larger post-1990 than pre-1960; however, because major hurricanes are relatively infrequent and have different tracks, widths, and propagation speeds, random chance may explain this observation. Hence, to test the hypothesis that increasing channel depths have amplified storm surge and storm tides, a numerical modeling approach is needed.

2.2. Data Sources

Hourly tide data used to validate the idealized tidal model were obtained from the National Oceanographic and Atmospheric Administration (NOAA) for Southport, NC (1976–1988 and 2006–2008) and Wilmington, NC (1935–2015). Nineteenth and early twentieth century hourly tabulations were photographed at the U.S. National Archives [see *Talke and Jay*, 2013] and digitized, including hourly data from Wilmington (1887–1888, 1890–1891, 1908–1912) and Southport (1923–1924). Further, hourly records from Southport (1933–1954) were recovered from the National Centers for Environmental Information (https://www.ncdc.noaa.gov/EdadsV2) and digitized. Harmonic constituents obtained from 12 short-term gauges are also used [*Welch and Parker*, 1979].

River discharge measurements by the United States Geological Survey (USGS) confirm that flood events generally do not coincide with hurricane storm surge. Since river discharge is generally small during hurricane events, we assume—to first order—that the system is well mixed [see *Becker et al*., 2010] and that nonlinear interactions between the river and storm tide are negligible. A barotropic modeling approach is therefore justified.

To estimate an idealized CFRE bathymetry, 23 cross-sectional profiles of depth were digitized in 2 km increments from an 1888 topographical map published by the U.S. Coast and Geodetic Survey, and a smooth, idealized bathymetry was fit to the cross sections (Figures 1 to 3; supporting information). A digital elevation model (DEM) of Cape Fear from 1975 was obtained from NOAA, and the 2015 channel depth was estimated from *Olsen* [2012]. Modeled depth and width changes are presented in the supporting information; compared to historical conditions, the modern cross-sectional area is 0–20% larger than historically, but the width is 0–20% smaller (see supporting information).

2.3. Hydrodynamic Model

A depth-averaged Delft3D numerical model [*Booij et al*., 1999] was configured with idealized depth and width variations that approximate the natural system in a least square sense (see supporting information). The along-channel variation in width is modeled as a Gaussian curve, which allows for an initial expansion in width between Rkm 0 and 12 and an exponential decrease between Rkm 12 and 50. The channel cross section is modeled as a Gaussian curve (Figure 2c) and is constrained to approximate the cross-sectional area as a function of river kilometer (see supporting information), allowing for both channel and shallow subtidal areas. The width convergence length scale (i.e., the length over which the width decreases by a factor of e) between Rkm 12 and 50 is 17 km and 20 km, respectively, for the historic (1888) and modern (1975 and 2015) models (see supporting information, Figure S3). Channel depths of 7 m, 13.25 m, and 15.5 m relative to mean sea level are applied for the 1888, 1975, and 2015 conditions, respectively. To allow damping of the tidal wave, the river is modeled with a constant width of 120 m and a constant depth of 4 m (for 1888) and 5 m (for 1975 and 2015) for 150 km upstream of Rkm 50.

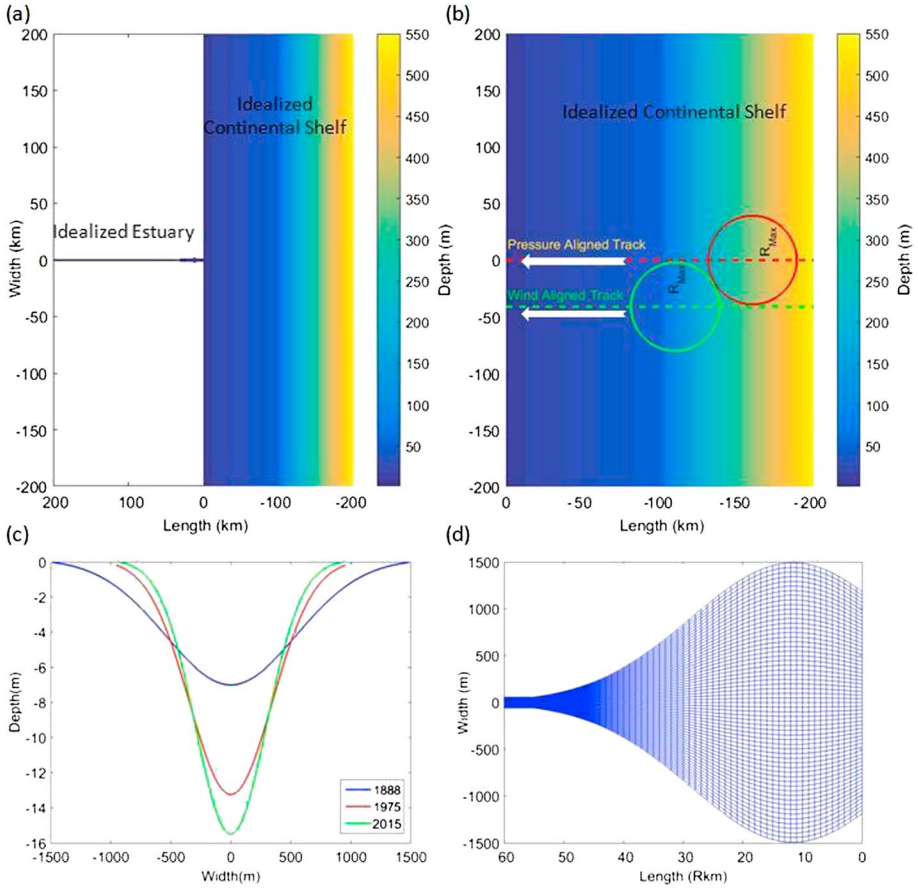

Figure 2. (a) Idealized model bathymetry, (b) the plan view of TC tracks on the continental shelf, which move from right to left (c) idealized channel cross-section at the mouth, and (d) the plan view of the first 60 km of estuary grid. The ocean/estuary boundary is at Rkm 0. Wind forcing is only included on the continental shelf (section 2.4).

Continental shelf topography is approximated from modern bathymetric measurements [*Olsen*, 2012] and slopes linearly downward from the coast to a depth of 550 m at 200 km offshore. Following observations on maps, the channel at the estuary mouth is extended 1.2, 4, and 5 km onto the shelf for the 1888, 1975, and 2015 conditions, respectively. Coastal geometry has been simplified to a straight coastline, and the estuary orientation has been made perpendicular to the coast. The length and width of the continental shelf model are 200 km and 400 km, respectively, which was found through sensitivity studies to be adequate

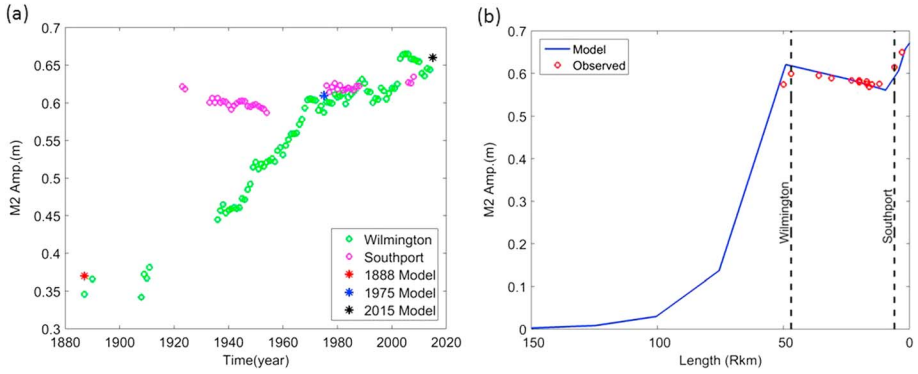

Figure 3. (a) Measured and modeled M2 amplitude at Wilmington and Southport over time and (b) variation of modeled M2 in the idealized "1975" estuary, compared against measurements. Zero is at the river entrance, and positive direction is landward to the left of the graph.

for simulating storm surge; doubling the domain size resulted in a less than 1% change in storm surge results. As shown below, the good agreement between measured and modeled tidal constituents validates the idealized approach. A total of 62 grids in the lateral direction and 273 in the along-channel direction are used in the estuary and 113 and 140 along the continental shelf.

The hydrodynamic model is forced at the seaward boundary by M2, S2, N2 (semidiurnal), and K1, O1, and P1 (diurnal) tidal constituents derived from the Oregon State University Tidal Inversion Software package [*Egbert and Erofeeva*, 2002]. River forcing at the landward end was set to 268 m^3/s, representing average conditions. Overland flooding and the effects of short-period waves (swell) are not considered.

2.4. Metrological Forcing

At least two approaches are typically used to model and analyze storm surge, defined here as the difference between the measured water level and predicted tide. Fully resolved, 2-D or 3-D hydrodynamic models with realistic meteorological forcing and coastal bathymetry are useful for understanding the effects of individual events on specific landscape features [e.g., *Orton et al*., 2012; *Colle*, 2003]. On the other hand, idealized, parametric hurricanes with simplified wind and pressure fields are often used to develop sensitivity studies that investigate nonlinear interactions or the effects of changing meteorological and hydrodynamic variables [e.g., *Shen and Gong*, 2009]. Idealized models require less computational time and reduce complexity, simplifying analysis and interpretation of physical processes. This enables an ensemble-based approach, in which a large parameter space is tested to help assess hazard probability [e.g., *Rumpf et al*., 2009]. For these reasons, we apply an idealized approach.

The parametric model of *Holland* [1980] was used to estimate the meteorological forcing during a tropical cyclone:

$$P = P_c + (P_n - P_c)\exp\left(-A/r^B\right) \tag{1}$$

$$V_w' = \left[AB(P_n - P_c)\exp\left(-A/r^B\right)/\left(\rho r^B\right)\right]^{1}/_{2} \tag{2}$$

where ρ is the air density, P_c is the hurricane central pressure (see supporting information Table S1), P_n is the ambient pressure, A and B are scaling parameters, P is the atmospheric pressure at radius r, and V'_w is the wind velocity. The parameter A is defined by $A = (R_{max})^B$, where R_{max} represents the distance from the storm center to the location of maximum wind and B is a constant with values between 1 and 2.5 [*Holland*, 1980]. Following *Hsu and Yan* [1998], we apply an R_{max} of 34, 34, 34, 46, 51, 48, and 47 km to represent a tropical depression (TD), tropical storm (TS), and hurricane categories 1–5, (Saffir-Simpson hurricane scale), respectively. The maximum wind speed and the center pressure ranged from 11.75 m/s and 998 mbar (TD) to 78.8 m/s and 910 mbar (CAT-5); see supporting information Table S1. The parameter B is defined to be 2.25.

To allow sufficient time for storm surge to develop and to test the worst-case scenario, we apply a storm track that moves perpendicularly to the coast with a translation speed of 18 km/h, representing a slow moving hurricane that injects more momentum into the water and can result in a higher storm tide [*Mei et al*., 2012]. The wind drag coefficient is modeled using the *Yelland and Taylor* [1996] equation for U_{10} and is capped at 0.003 for wind speeds larger than 30 m/s [see *Powell et al*., 2003 and *Donelan et al*., 2004]. Because the actual CFRE is at an oblique angle to the coast (Figure 1), actual storm tracks with a perpendicular approach will veer away from the estuary centerline; moreover, hurricane magnitudes decrease upon landfall. For both of these reasons, we assume that the estuary-generated portion of storm surge for a perpendicularly oriented storm is negligible compared to the coastal component and apply TC forcing only over the continental shelf. This simplification means that we are essentially testing how an externally forced storm surge behaves in the estuary, rather than a continually forced long wave. The consequences of this assumption are investigated using sensitivity studies and discussed later.

2.5. Model Calibration and Validation

The idealized model was calibrated by adjusting the Chezy bed friction coefficient until the modeled progression of the dominant M2 tide over a 40d run matched observations from 1976 (Figure 3b). A Chezy coefficient of 23 and 65 was applied for the estuary and the continental shelf, respectively, and yielded an RMS error of 0.013 m. The relatively large bed friction (small Chezy coefficient) within the estuary likely compensates for unmodeled roughness features such as marsh vegetation and/or variations in bathymetry. The spatially constant bed friction coefficients were then applied, unchanged, to the 1888 and 2015 models. Harmonic

analysis [e.g., *Leffler and Jay*, 2009] shows that the modeled constituents for the 1888, 1975, and 2015 conditions compare favorably with tide records in Wilmington and Southport (Figure 3a). Therefore, despite simplifications, our idealized model reproduces the observed secular trends in the CFRE and is capturing the first-order behavior of long waves in the real system.

2.6. Sensitivity Studies

To investigate changing conditions, a total of 546 model runs were carried out on the calibrated model domain, representing three time periods (1888, 1975, and 2015), seven storm intensities (from TD to CAT-5), two storm tracks, and 13 tidal phases ($3 \times 7 \times 2 \times 13 = 546$). Two types of storm tracks are modeled for each storm intensity: wind aligned, in which the maximum wind speed coincides with and travels along the estuary center axis, and pressure aligned, in which the eye of the hurricane coincides with and travels along the estuary center axis (Figure 2b). Further, each track/intensity/year combination is run an additional 13 times, with the timing of the storm spaced in 1 h increments over the tidal cycle. In this way the effects of depth changes (e.g., high or low tide) and current direction (either opposed or collinear with wind-induced currents) are assessed. The parametric storms were applied during mean tidal conditions (halfway between spring and neap). Storm surge was estimated from the modeled storm tide by subtracting out the tide from the calibration runs.

3. Results and Discussion

Analysis of archival data indicates that the M2 amplitude in Wilmington has nearly doubled over the past century, from ~0.35 m in the late nineteenth/early twentieth century to ~0.65 m today (Figure 3a). Over a similar period, the M2 amplitude near the coast (Southport) has increased only slightly. Similarly, tidal range in Wilmington has doubled to 1.55 m since the 1880s, with a much smaller increase of 0.07 m observed in Southport since the 1920s (see Figure S5). Clearly, the divergence in observed tidal amplification in these locations suggests that changes to the estuary physics, rather than the ocean, explains most of the secular changes at Wilmington. In fact, the observed changes in tides are reproduced by changing only the depth and width of the modeled channel (Figure 2c). Further sensitivity studies suggest that depth changes are primarily responsible. When only depth is changed between the 1888 and 1975 models, the greater diurnal tide range (GDR) increases from 0.86 to 1.57 m. When width changes are also included (default condition; see supporting information Figure S3), GDR increased an additional 0.11 m, to 1.68 m. These results suggest that the majority of the observed tidal (long-wave) changes are produced by depth changes, rather than width variability caused by dredging or shoreline changes.

Idealized TC runs also suggest that a deeper system will produce a greater storm tide and storm surge, for the same meteorological forcing (Figure 4). For the "wind-aligned" scenario with 1888 depth, storm surge at Wilmington (Rkm 47) is modeled to be 0.7 ± 0.15 m and 3.8 ± 0.25 m for a CAT-1 and CAT-5, respectively (Figure 4c), with the observed variability around the mean caused by different timing relative to tidal phase. By contrast, the deeper 2015 scenario produces storm surges of 1.2 ± 0.45 m and 5.6 ± 0.6 m for a CAT-1 and CAT-5, respectively (Figure 4c). Similarly, the modeled CAT-5 storm tide in 2015 is 1.65 ± 0.25 m and 0.95 ± 0.18 m larger than the 1888 simulations in the wind-aligned and pressure-aligned scenarios, respectively (Figures 4a and 4b). Overall, modeled storm surge and storm tide heights at Wilmington increased between the 1888 and 2015 models for all modeled TCs, such that there is almost no overlap in the range of modeled heights. A less drastic change is modeled between the 1975 and 2015 scenarios, likely due to a smaller proportional increase in depth. For reference, the National Weather Service considers a storm tide of 2.04 m (6.7 feet) to be the threshold for moderate flooding in Wilmington (horizontal dashed line in Figures 4a and 4b). Hence, modeling results suggest that the number of storms that can cause significant surge and flooding has likely increased over time. Measurements at Wilmington qualitatively support this conclusion; the largest five storm surges on record all occurred since 1980 (Figures 4c and 4d).

Between the ocean and Wilmington, the spatial progression in surge amplitude closely follows the pattern of the M2 tide (Figure 3b). In the 1888 simulations, storm surge (like tides) decreased by nearly a factor of 2 between Rkm 0 and Rkm 50, whereas in the 2015 simulation amplitudes are nearly the same (see Figure S7 in the supporting information). Sensitivity studies show that river flow has a minor, though important, effect on surge amplitudes at Wilmington. For example, increasing river flow to 1000 m^3/s decreases the CAT-1 storm

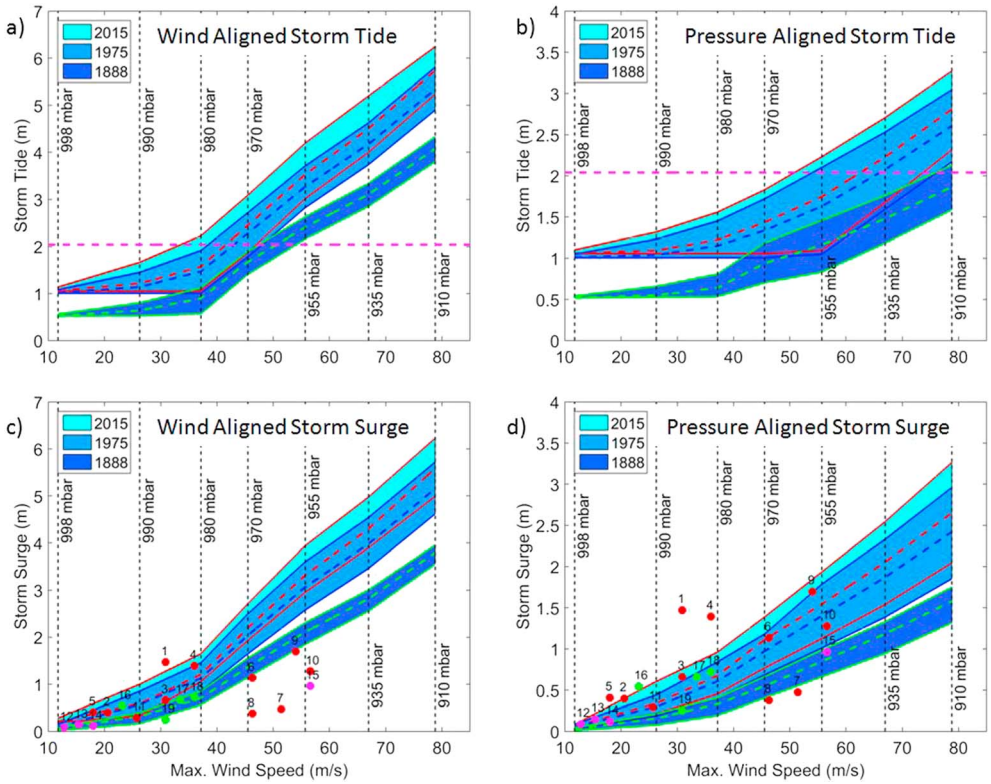

Figure 4. (a–d) Modeled storm tide and storm surge at Wilmington (Rkm 47) produced by seven different TC strengths, varying from TD to CAT-5. The vertical dashed lines indicate barometric pressure and peak wind speeds of the modeled TC on the continental shelf domain. The fill areas around the mean shows the range of results obtained from 13 hourly spaced tidal phases. Red, magenta, and green circles show measured TCs from 1980–present, 1950–1980, and pre–1950, respectively, and include (1) Hurricane Hanna (2008), (2) Hurricane Barry (2007), (3) Hurricane Ernesto (2006), (4) Hurricane Charley (2004), (5) Hurricane Kyle (2002), (6) Hurricane Floyd (1999), (7) Hurricane Bonnie (1998), (8) Hurricane Bertha (1996), (9) Hurricane Fran (1996), (10) Hurricane Diana (1984), (11) Hurricane Dennis (1981), (12) unnamed (1972), (13) Hurricane Abby (1968), (14) unnamed (1961), (15) Hurricane Hazel (1954), (16) unnamed (1946), (17) unnamed (1945), (18) unnamed (1944), and (19) unnamed (1910). Vertical scales are different between wind and pressure-aligned graphs. The horizontal magenta dashed lines in Figures 4a and 4b represent the National Weather Service threshold for moderate flooding in Wilmington of 2.04 m.

surge from 1.12 m to 1.04 m in the 1975 simulation (not shown). However, since flow events stemming from TCs typically occur, many days after the storm surge, such elevated flow conditions are unlikely.

Several factors drive increased storm tides in the modern simulations. First, increases in mean high water have resulted in a larger possible storm tide, independent of meteorological forcing. This effect is especially prominent for low-energy storms like tropical depressions, in which the increase in the peak water level from 0.55 to 1.05 m between the 1888 and 2015 scenarios is almost entirely driven by larger tides (Figures 4a and 4b). A large tide range also contributes to the greater variability (spread) in storm tide heights observed in modern model runs.

We also posit that both tides and storm tides have increased because channel deepening reduces the hydraulic resistance to incoming long waves [e.g., *Chernetsky et al*., 2010]. In analytical models of tide propagation, the friction term in the momentum equation is linearized to be proportional to C_d/H, where C_d is the linearized drag coefficient and H is the depth [e.g., *Jay*, 1991; *Friedrichs and Aubrey*, 1994]. Hence, doubling depth over the past century has a similar dynamic effect on a tide wave as halving friction. Decreasing shoreline width between levees, as modeled here, will also amplify tides [*Jay*, 1991]. Since the estuary is strongly convergent upstream of Rkm 12, an incoming wave is characterized by a balance between smaller cross sections (tending to amplify) and bed friction (tending to damp). Increased depth alters this balance and helps explain why both tides and storm tides have amplified over time. Scaling of momentum terms in model results also indicates that inertial effects (du/dt) are important and have become more prominent over time.

Unlike some estuaries such as the Ems [*Chernetsky et al*., 2010], traditional quarter wave resonance does not appear to play a role here since the deep channel is only 50 km long, smaller than the quarter wave wavelength. However, sensitivity studies suggest that wave celerity and M2 phase change at the transition from the shipping channel (15.5 m depth) to the river channel (5 m) upstream of Wilmington, suggesting that some wave reflection is occurring that may contribute to the modeled water levels.

Compared to historical events, the modeled storm surge from wind-aligned conditions often exceeds observed magnitudes at Wilmington (Figure 4c), particularly for larger storms. Since no historical storm tracks are exactly wind aligned, and storms often lose power near the shore, this result is not unexpected (see supporting information). On the other hand, some measured events exceed the pressure-aligned model experiments (Figure 4d), which show that the order of magnitude of simulation results (Figure 4) is plausible. The overall consistency with actual tide and storm tide measurements demonstrates that the model experiments likely capture the correct historical trend. The wind-aligned scenario can be interpreted as the worst-case scenario: though most historical storms approach the CFRE at some angle and have made landfall elsewhere, a perpendicular approach is not implausible (as hurricane Sandy showed in NJ). When meteorological forcing in the estuary is included, sensitivity studies suggest that overall storm tide magnitudes increase and that the differences between the 1888 and 2015 scenarios decrease by as much as 0.35 m in a CAT-5 event (not shown). Therefore, preliminary results suggest that the local, estuary contribution to surge has decreased over time (due to increasing depth) but not enough to compensate for the amplification in the externally forced wave.

The idealized modeling results support the hypothesis that significant change has occurred in both tides and storm tides due to channel deepening. To fully assess changed magnitudes and flood risk, a fully realized numerical model is required that includes more complex bathymetry, variable friction linked to bed types, more realistic storm forcing, different propagation speeds, wetlands and other intertidal areas, overland flow and flooding effects, and periodic estuary stratification. In particular, large-scale overland flooding (the levee-break scenario) may reduce the predicted storm surge heights in the extreme scenarios and hence the modeled change over time. Bathymetric changes due to sea level rise and erosion/sedimentation processes, though small compared to historical channel deepening, may also have affected tides and storm surge. An ensemble of storm tracks and storm characteristics should be modeled to fully understand how the worst-case scenario has changed over time. Nonetheless, results validate the hypothesis that direct anthropogenic interventions are the primary cause of both changed tidal and storm surge dynamics in the CFRE. Since we did not consider the natural, pre-1850 condition of a 3–5 m deep estuary, historical changes may be more extreme than suggested. For all these reasons, further investigation with realistic bathymetry is warranted to constrain the change in flood hazard in Wilmington (NC).

4. Conclusions

In this study we develop an idealized numerical model to investigate how changing channel depths affect tides and storm surge in the CFRE. Model results suggest that tide propagation into the system has been strongly affected by increases in channel depth from 7 m to 15.5 m over the last 130 years, leading to a doubling of tidal range in Wilmington. The anthropogenically altered bathymetry also increases the modeled storm surge: the same tropical cyclone making landfall today will produce significantly larger water levels than in the nineteenth century. Since many harbors worldwide have been deepened since the nineteenth century, and because many locations worldwide exhibit substantial trends in tidal properties [*Woodworth*, 2010; *Mawdsley et al*., 2015], it is probable that a secular change in storm surge risk has also occurred in other estuaries, to an extent related to tide changes. In the future, local depth changes due to accelerating sea level rise [*Church et al*., 2013] and additional development may further alter storm surge characteristics and flood hazard.

Acknowledgments
Funding was provided by the Office of Naval Research (award N00014-13-1-0084), the U.S. Army Corps of Engineers (Award W1927N-14-2-0015), and the National Science Foundation, award 1455350. We thank M. Al-Murib and Sam Hawkinson, for digitizing the archival tide data, and D. Jay for helpful discussions on tides. Tide data were obtained from the NOAA, the U.S. National Archives, and the National Centers for Environmental Information. River discharge measurements were obtained from the USGS. The CFRE 1888 topographical map and the DEM of Cape Fear from 1975 were obtained from the U.S. Coast and Geodetic Survey and NOAA. The authors would like to thank two anonymous reviewers for their beneficial comments, which helped improve the manuscript.

References

Becker, M. L., R. A. Luettich, and M. A. Mallin (2010), Hydrodynamic behavior of the Cape Fear River and estuarine system: A synthesis and observational investigation of discharge-salinity intrusion relationships, *Estuarine Coastal Shelf Sci.*, *88*(3), 407–418, doi:10.1016/j.ecss.2010.04.022.

Booij, N., R. C. Ris, and L. H. Holthuijsen (1999), A third-generation wave model for coastal regions: 1. Model description and validation, *J. Geophys. Res.*, *104*, 7649, doi:10.1029/98JC02622.

Chernetsky, A. S., H. M. Schuttelaars, and S. A. Talke (2010), The effect of tidal asymmetry and temporal settling lag on sediment trapping in tidal estuaries, *Ocean Dynam.*, *60*(5), 1219–1241, doi:10.1007/s10236-010-0329-8.

Church, J. A., et al. (2013), Sea level change, in *Climate Change 2013: The Physical Science Basis. Contribution of Working Group I to the Fifth Assessment Report of the Intergovernmental Panel on Climate Change*, edited by T. F. Stocker et al., Cambridge Univ. Press, Cambridge, and New York.

Climate Change Science Program Synthesis and Assessment Product 4-7 (2008), Impacts of climate change and variability on transportation systems and infrastructure: Gulf coast study.

Colle, B. A. (2003), Numerical simulations of the extratropical transition of Floyd (1999): Structural evolution and responsible mechanisms for the heavy rainfall over the northeast united states, *Mon. Weather Rev.*, *131*(12), 2905–2926, doi:10.1175/1520-0493(2003)131<2905:NSOETE>2.0.CO;2.

Donelan, M. A., B. K. Haus, N. Reul, W. J. Plant, M. Stiassnie, H. C. Graber, O. B. Brown, and E. S. Saltzman (2004), On the limiting aerodynamic roughness of the ocean in very strong winds, *Geophys. Res. Lett.*, *31*, L18306, doi:10.1029/2004GL019460.

Egbert, G. D., and S. Y. Erofeeva (2002), Efficient inverse modeling of barotropic ocean tides, *J. Atmos. Oceanic Technol.*, *19*(2), 183–204, doi:10.1175/1520-0426(2002)019<0183:EIMOBO>2.0.CO;2.

Friedrichs, C. T., and D. G. Aubrey (1994), Tidal propagation in strongly convergent channels, *J. Geophys. Res.*, *99*, 3321–3336, doi:10.1029/93JC03219.

Giese, G. L., H. B. Wilder, and G. G. Parker (1985), Hydrology of major estuaries and sounds of North Carolina, United States Geological Survey Water-Supply, (8.1).

Grinsted, A., J. C. Moore, and S. Jevrejeva (2012), Homogeneous record of Atlantic hurricane surge, *Proc. Natl. Acad. Sci. U.S.A.*, *109*(48), 19,513–19,514, doi:10.1073/pnas.1216735109.

Holland, G. J. (1980), An analytic model of the wind and pressure profiles in hurricanes, *Mon. Weather Rev.*, doi:10.1175/1520-0493(1980)108<1212:AAMOTW>2.0.CO;2.

Holland, G. J., and P. J. Webster (2007), Heightened tropical cyclone activity in the North Atlantic: Natural variability or climate trend?, *Philos. Trans. R Soc. A.*, *365*(1860), 2695–2716.

Hsu, S. A., and Z. Yan (1998), A note on the radius of maximum wind for hurricanes, *J. Coast. Res.*, *14*(2), 667–668. [Available at from http://www.jstor.org/stable/4298820.]

Jay, D. A. (1991), Green's law revisited: Tidal long-wave propagation in channels with strong topography, *J. Geophys. Res.*, *96*, 20,585, doi:10.1029/91JC01633.

Kemp, A. C., and B. P. Horton (2013), Contribution of relative sea-level rise to historical hurricane flooding in New York City, *J. Quat. Sci.*, *28*(6), 537–541.

Landsea, C. W., G. A. Vecchi, L. Bengtsson, and T. R. Knutson (2010), Impact of duration thresholds on Atlantic tropical cyclone counts, *J. Clim.*, *23*, 2508–2519, doi:10.1175/2009JCLI3034.1.

Lanzoni, S., and G. Seminara (1998), On tide propagation in convergent estuaries, *J. Geophys. Res.*, *103*, 30,793–30,812, doi:10.1029/1998JC900015.

Leffler, K. E., and D. A. Jay (2009), Enhancing tidal harmonic analysis: Robust (hybrid L1/L2) solutions, *Cont. Shelf Res.*, *29*(1), 78–88, doi:10.1016/j.csr.2008.04.011.

Lin, N., K. Emanuel, M. Oppenheimer, and E. Vanmarcke (2012), Physically based assessment of hurricane surge threat under climate change, *Nat. Clim. Change*, *2*, 462–467, doi:10.1038/nclimate1389.

Ludlam, D. M. (1963), *Early American Hurricanes, 1492–1870*, 198 pp., Am. Meteorol. Soc., Boston, Mass.

Mawdsley, R. J., I. D. Haigh, and N. C. Wells (2015), Global secular changes in different tidal high water, low water and range levels, *Earth's Future*, 1–16, doi:10.1002/2014EF000282.

Mei, W., C. Pasquero, and F. Primeau (2012), The effect of translation speed upon the intensity of tropical cyclones over the tropical ocean, *Geophys. Res. Lett.*, *39*, L07801, doi:10.1029/2011GL050765.

Olsen Associates Inc. (2012), Calibration of a Delft3D model for Bald Head Island and the Cape Fear River entrance phase 1, 6114(April).

Orton, P., N. Georgas, A. Blumberg, and J. Pullen (2012), Detailed modeling of recent severe storm tides in estuaries of the New York City region, *J. Geophys. Res.*, *117*, C09030, doi:10.1029/2012JC008220.

Orton, P., S. Talke, D. Jay, L. Yin, A. Blumberg, N. Georgas, and K. MacManus (2015), Channel shallowing as mitigation of coastal flooding, *J. Mar. Sci. Eng.*, *3*(3), 654–673, doi:10.3390/jmse3030654.

Peng, M., L. Xie, and L. J. Pietrafesa (2004), A numerical study of storm surge and inundation in the Croatan–Albemarle–Pamlico Estuary System, *Estuarine Coastal Shelf Sci.*, *59*(1), 121–137, doi:10.1016/j.ecss.2003.07.010.

Powell, M. D., P. J. Vickery, and T. A. Reinhold (2003), Reduced drag coefficient for high wind speeds in tropical cyclones, *Nature*, *422*(6929), 279–283, doi:10.1038/nature01481.

Prandle, D. (2003), Relationships between tidal dynamics and bathymetry in strongly convergent estuaries, *J. Phys. Oceanogr.*, *33*(12), 2738–2750, doi:10.1175/1520-0485(2003)033<2738:RBTDAB>2.0.CO;2.

Rumpf, J., H. Weindl, P. Höppe, E. Rauch, and V. Schmidt (2009), Tropical cyclone hazard assessment using model-based track simulation, *Nat. Hazards*, *48*(3), 383–398, doi:10.1007/s11069-008-9268-9.

Shen, J., and W. Gong (2009), Influence of model domain size, wind directions and Ekman transport on storm surge development inside the Chesapeake Bay: A case study of extratropical cyclone Ernesto, 2006, *J. Mar. Syst.*, *75*(1-2), 198–215, doi:10.1016/j.jmarsys.2008.09.001.

Shen, J., H. Wang, M. Sisson, and W. Gong (2006), Storm tide simulation in the Chesapeake Bay using an unstructured grid model, *Estuarine Coastal Shelf Sci.*, *68*(1), 1–16, doi:10.1016/j.ecss.2005.12.018.

Talke, S. A., and D. A. Jay (2013), Nineteenth century North American and Pacific tidal data: Lost or just forgotten?, *J. Coast. Res.*, *29*(6A), 118–127, doi:10.2112/JCOASTRES-D-12-00181.1.

Talke, S. A., P. Orton, and D. A. Jay (2014), Increasing storm tides in New York Harbor, 1844–2013, *Geophys. Res. Lett.*, *41*, 3149–3155, doi:10.1002/2014GL059574.

USACE COE, (1873), Report of the Secretary of War, Annual Report of the Chief of Engineers to the Secretary of War for the fiscal year ending June 30, 1873, Appendix T20-T21, U.S. Govt. Print. Off., Washington, D. C.

USACE COE, (1915), Report of the Secretary of War, Annual Report of the Chief of Engineers for historical summary giving the scope of previous projects for the improvement of certain rivers and harbors, U.S. Govt. Print. Off., Washington, D. C.

Wamsley, T. V., M. A. Cialone, J. M. Smith, J. H. Atkinson, and J. D. Rosati (2010), The potential of wetlands in reducing storm surge, *Ocean Eng.*, *37*(1), 59–68, doi:10.1016/j.oceaneng.2009.07.018.

Welch, J. M., and B. Parker (1979), NOAA Technical Report—Circulation and hydrodynamics of the lower Cape Fear River, North Carolina, pp. 1–18.

Woodworth, P. L. (2010), A survey of recent changes in the main components of the ocean tide, *Cont. Shelf Res.*, *30*(15), 1680–1691, doi:10.1016/j.csr.2010.07.002.

Xia, M., L. Xie, L. J. Pietrafesa, and M. Peng (2008), A numerical study of storm surge in the Cape Fear River Estuary and adjacent coast, *J. Coast. Res.*, *24*(4C), 159–167.

Yelland, M., and P. K. Taylor (1996), Wind stress measurements from the open ocean, *J. Phys. Oceanogr.*, doi:10.1175/1520-0485(1996)026<0541:WSMFTO>2.0.CO;2.